J Mater Sci (2007) 42:5360–5368
DOI 10.1007/s10853-006-0891-0

# Numerical model for nucleation of peritectic alloy during unidirectional solidification

**Yunpeng Su · Meng Wang · Xin Lin · Qian Chen · Weidong Huang**

Received: 17 February 2006 / Accepted: 25 August 2006 / Published online: 29 March 2007


**Abstract** Based on transient nucleation theory, a numerical model has been constructed to describe the nucleation process of a new phase in front of the liquid–solid interface of a prior steady-growth phase in peritectic alloy with the combination of the concentration field calculated by a self-consistent numerical model for cellular/dendritic growth. The results show that the nucleation incubation time of a new phase varies with the solidification rate during unidirectional solidification. During unidirectional solidification of the Zn–4.0 wt.% Cu alloy, the incubation time changes very slightly when the solidification rate increases from 50 to 500 μm/s, but it increases significantly when the solidification rate exceeds 500 μm/s. The calculated results show a reasonable agreement with the experimental ones. This model reveals that nucleation of a new phase is time-dependent and reasonably explains the effect of the solidification velocity on the behaviors of nucleation and growth of ε dendrites in the matrix of the $\eta$ phase in unidirectional solidification of Zn rich Zn–Cu alloys.

Y. Su · M. Wang · X. Lin · W. Huang
State Key Laboratory of Solidification Processing, Northwestern Polytechnical University, Xi'an 710072, P.R. China

Q. Chen
College of Foreign Language, Lan Zhou University of Technology, Lanzhou 730050, P.R. China

Y. Su (✉)
Department of Industrial and Systems Engineering, The Hong Kong Polytechnic University, Hung Hom, Kowloon, Hong Kong
e-mail: zhangyangqiansyp@yahoo.com.cn

## Introduction

Solidification of materials includes two important stages, i.e. nucleation and growth. In general, nucleation is treated as an important control factor of the microstructural selection in undercooled solidification of peritectic materials. Nucleation of the primary and peritectic phases in bulk melts of Fe–C [1], Sn–Sb [2] and Al–Ti [3] alloys was studied at rather low cooling rates in 1970s. In the last decade, the high undercooling technique was introduced into the nucleation research to investigate the selection of stable and metastable phases of peritectic alloys under non-equilibrium conditions. Via this technique, some new phenomena, such as direct nucleation of metastable phases from the melt, were observed [4–6]. However, there were much fewer experimental researches on the nucleation in peritectic alloys under unidirectional solidification. Ma et al. [7] observed equiaxed ε dendrites in the matrix of the $\eta$ phase during unidirectional solidification of Zn rich Zn–Cu alloys. In our previous paper [8], Wang et al. quantitatively measured the critical solidification rate at which these equiaxed ε dendrites disappeared in the same alloys and calculated the constitutional undercooling for the ε phase nucleating in front of a prior steady-growth interface. But there still lacks a good understanding on the fact that these equiaxed ε dendrites will disappear even if the ε phase still has large enough undercooling to nucleate heterogeneously.

In 1942, considering nucleation as a process determined by the activated state of the systemic ambient phase, Zeldovich [9] formulated a generalized version of the kinetics of first order phase transitions and obtained the first fundamentally correct solution for the kinetics of forming crystal nuclei. These solutions showed that nucleation is a transient process and determined by the time lag of the

nucleation process, $\tau^{\#}$. $\tau^{\#}$ is the time interval spent by the nucleating system on reaching a steady-state distribution of growing clusters, i.e. a steady-state nucleation rate. In 1976, Binder and Stauffer [10] introduced another characteristic time $\Delta t_p$, which is the time spent by the clusters of the new phase on reaching a perceptible size [11]. It built a correlation between the transient nucleation theory established by Zeldovich and the experimental observations. Up to now, Zeldocich model has been widely employed to evaluate the kinetic stability of undercooled liquids and their glass-forming abilities [12–14], investigate the influence of the kinetics of non-steady-state heterogeneous nucleation on the glass-formation abilities of ceramic materials [15], and explore the effect of undercooling on the formation of metastable phases during high undercooling rapid solidification [4, 16]. In 1993, Kelton [17] developed a numerical model to describe the transient nucleation process in lithium disilicate, a model glass, and it showed a reasonable agreement with the DSC data.

In this paper, a numerical model has been developed to simulate the nucleation process of a new phase in front of a steady-growth interface in peritectic alloys during unidirectional solidification. The calculated results were compared with the experimental results of unidirectionally solidified Zn rich Zn–Cu peritectic alloys. The binary phase diagram of Zn-rich Zn–Cu alloys was shown in Fig. 1.

## Formulation of the model

### Self-consistent model for cells/dendrites

Before the nucleation behavior of a new phase in front of a steady growth interface can be simulated, temperature and concentration fields in the liquid phase and the shape of the solid/liquid interface should be solved. So in the present paper, a self-consistent numerical model for single-phase solidification represented in our previous papers [19, 20] was applied to obtain a self-consistent interface with quantitatively defined temperature and concentration fields in front of it.

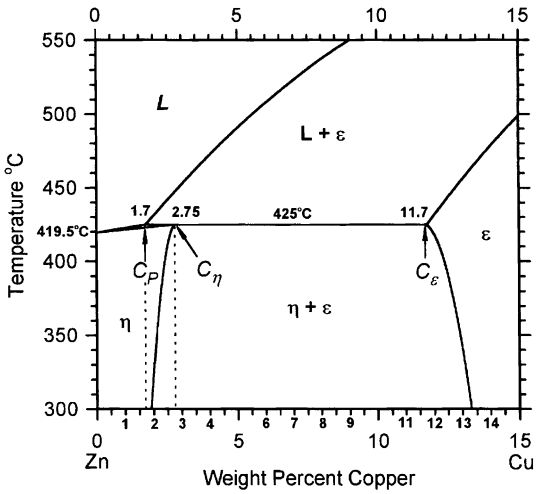


**Fig. 1** Binary phase diagram of Zn-rich Zn–Cu alloys [18]

Considering an axisymmetric interface shape and neglecting the effect of convection currents, we set a moving coordinate system fixed to the experimental sample during unidirectional solidification. Usually, the solidification latent heat is small and the heat conductivity is large, so the temperature field is assumed to be linear. Then the temperature field is defined as

$$T_i = T_0 + G_T z, \tag{1}$$

where $T_0$ is the liquidus temperature of the mean composition, $C_0$, $G_T$ is the imposed temperature gradient at the interface, $z$ is the axial position in the coordinate system moving at the pulling velocity, $V_0$, and this coordinate system is referred to as the gradient coordinate system. The solute distributions in the liquid and solid are determined by the following diffusion equations corresponding to the above moving coordinates, respectively:

$$D_L \nabla^2 C_L + V_0 \frac{\partial C_L}{\partial z} = \frac{\partial C_L}{\partial t} \tag{2}$$

$$D_S \nabla^2 C_S + V_0 \frac{\partial C_S}{\partial z} = \frac{\partial C_S}{\partial t}, \tag{3}$$

where $C_L$, $C_S$ are the solute concentrations for the liquid and solid phases and $D_L$, $D_S$ are the solute diffusivities for the liquid and solid phases, respectively. The solute concentrations for the liquid and solid phases should also satisfy the following far field conditions:

$$C_L = C_0, \quad \text{at } z \to +\infty \tag{4}$$

$$\frac{\partial C_S}{\partial z} = 0, \quad \text{at } z \to -\infty. \tag{5}$$

At the interface:

$$C_{Si} = kC_{Li} \tag{6}$$

$$V_n(k-1)C_{Li} = D_L \frac{\partial C_L}{\partial n} - D_S \frac{\partial C_S}{\partial n}, \tag{7}$$

where $V_n$ is the growth velocity in the normal direction and $k$ is the distribution coefficient, respectively.

The temperature and concentration fields at the interface must satisfy the Gibbs–Thomson equation

$$T_i = T_0 + m(C_{\mathrm{Li}} - C_0) - \Gamma\left(\zeta\frac{1}{R_1} + \frac{1}{R_2}\right) - \frac{V_n}{\mu}, \qquad (8)$$

where $\xi = 1–\alpha_n\cos(n\theta)$, $\theta$ is the angle between the interfacial normal and the dendrite growth direction, $n$ is the rotational symmetry degree of the alloy crystal lattice, $\alpha_n$ is the anisotropic coefficient (As the two solid phases involved in Zn rich Zn–Cu peritectic alloys, i.e. ε and $\eta$ phases, are all non-facet phases, the anisotropy of them can be neglected. Consequently, $\alpha_n$ was set to 0 in the present paper.), $\Gamma$ is the Gibbs–Thompson coefficient, $R_1$ and $R_2$ are the main curvature radii at the interface, $\mu = V_C\Delta S_m/(R_g T_i)$ is the kinetic coefficient, $V_C$ is the upper limit of the crystalline growth velocity, $\Delta S_m$ is the fusion entropy, $R_g$ is the gas constant, $m = m_e(1 + (k_e–k(1–\ln k/k_e))/(1–k_e)$ is the non-equilibrium liquidus slope, and $m_e$ is the equilibrium liquidus slope, respectively.

Given a proper initial interface shape, the diffusion equations (2–7) were solved by using the finite-difference method through the control volume integration discretization technique. A self-consistent interface shape was obtained by coupling the temperature field with the solute field along the solid/liquid interface through Eq. 8. Based on the fact that the dendritic arrays in unidirectional solidification usually have a hexagonal structure of axial symmetry, only a symmetry unit of a dendrite, i.e. half of a dendrite unit, was taken into consideration in numerical calculations. The results of the above model included the concentration distribution in both the liquid and solid phases and some major morphological factors, such as the tip undercooling, the tip radius, the primary spacing, the stable shape of the dendrite, etc.

Then, for a new phase which possibly nucleates in front the solidification interface, the undercooling of each grid point in the liquid phase can be described as follows:

$$\Delta T' = T_l' - T_i = T_m' + m'C(x,z) - (T_0 - G_T z) \qquad (9)$$

where $C(x, z)$ is the concentration at the grid point $(x, z)$, $T_l'$ is the liquidus temperature of the new phase with a concentration of $C(x, z)$, $T_m'$ is the melting point of the pure new phase, $m'$ is the liquidus slope of the new phase, respectively. The relevant parameters were listed in Table 1.

**Table 1** Parameters for Zn–Cu diagram and thermophysical data of the phases involved solidification procedure

| Parameters | Symbol | Value | References |
|---|---|---|---|
| Melting point of Zn | $T_{Zn}$ | 692.73 K | [21] |
| Melting point of Cu | $T_{Cu}$ | 1358.02 K | [21] |
| Gibbs–Thompson coefficient of ε phase | $\Gamma_\varepsilon$ | $1.1 \times 10^{-7}$ K m | [22] |
| Gibbs–Thompson coefficient of $\eta$ phase | $\Gamma_\eta$ | $1.1 \times 10^{-7}$ K m | [22] |
| Equilibrium distribution coefficient of ε phase | $k_\varepsilon$ | 0.65 | [21] |
| Equilibrium distribution coefficient of $\eta$ phase (corrected) | $k_\eta$ | 0.62 | [21] |
| Peritectic temperature | $T_p$ | 698.14 K | [22] |
| Liquid composition at peritectic reaction | $C_l$ | 1.7 wt.%Cu | [22] |
| Diffusion coefficient in liquid at peritectic temperature | $D_L^*$ | $2.04 \times 10^{-9}$ m$^2$/s | [21] |
| Diffusion coefficient in solid at peritectic temperature | $D_S^*$ | $1.59 \times 10^{-12}$ m$^2$/s | [23] |
| Composition in primary ε at peretectic reaction | $C_\varepsilon$ | 11.7 wt.%Cu | [21] |
| Composition in peritectic $\eta$ at peretectic reaction | $C_\eta$ | 2.75 wt.%Cu | [21] |
| Equilibrium liquidus slope of ε phase | $m_e\varepsilon$ | –17.1 K/wt.%Zn | [21] |
| Equilibrium liquidus slope of $\eta$ phase | $m_e\eta$ | –3.19 K/wt.%Zn | [21] |
| Limit of crystalline growth velocity of ε phase | $V_{0\varepsilon}$ | 4,304 m/s | [24] |
| Limit of crystalline growth velocity of $\eta$ phase | $V_{0\eta}$ | 4,243 m/s | [24] |

## Transient nucleation model

It is known that crystal nuclei will exist in the liquid phase if the temperature of the liquid phase is below the corresponding liquidus line. Consequently, crystal nuclei of the new phase will generate in the liquid phase in front of the solid/liquid interface as long as there is a constitutional undercooling zone for this phase. On considering a convection-free condition, these crystal nuclei stay still in the liquid phase. It means that the solid/liquid interface moves towards these crystal nuclei at a velocity of $V_s$ (equal to $V_0$ under the steady-state condition) during unidirectional solidification. As mentioned in the Eq. 9, the constitutional undercooling for the new phase, $\Delta T'$, is a function of the axial position in the moving coordinate system, $z$. As a result, the constitutional undercooling of these crystal nuclei will change while the interface moves towards them. Under the steady-state condition discussed here, the axial position is just a function of time. Therefore, the nucleation of the new phase can be described as a non-isothermal crystallization process with a given temperature-variation rule determined by the applied solidification condition ($G$, $V_s$) for a given alloy. If we employ the classical nucleation theory to solve this problem, we will find that this approach is unsuitable for such a non-isothermal problem. Especially, when $V_0$ is higher than 1 mm/s, the corresponding variation rate of $\Delta T'$ is above 50 K/s. In such a condition, the strong time dependence of the nucleation rate and the rapid temperature-variation rate made it difficult to obtain a

cogent solution by employing the classical nucleation theory. Consequently, a numerical transient nucleation model similar to the one developed by Kelton [25] was adopted in the present paper.

Several simplifying assumptions have been made for the present model. First, spherical clusters of the nucleation phase have the same concentration as the liquid, i.e., a polymorphic crystallization is assumed. Second, stress is believed to relax quickly on the timescale of the crystal transformation and therefore ignored. Finally, a sharp interface between the cluster and the liquid phase is assumed and the thermodynamics of small clusters are derived from macroscopic thermodynamic parameters.

Clusters are assumed to evolve slowly in size by a series of bimolecular reactions [9]:

$$E_{n-1} + E_1 \underset{k_n^-}{\overset{k_{n-1}^+}{\Leftrightarrow}} E_n \tag{10}$$

$$E_n + E_1 \underset{k_{n+1}^-}{\overset{k_n^+}{\Leftrightarrow}} E_{n+1}, \tag{11}$$

where $E_n$ represents a cluster of $n$ molecules and $E_1$ represents a single molecule. Here, $k_n^+$, the rate of monomer addition to a cluster of $n$ molecules, and $k_n^-$, the rate of subtraction, are given by:

$$k_n^+ = \frac{24n^{2/3}D}{\lambda^2}\exp\left(-\frac{\delta g_n}{2k_BT}\right) \tag{12a}$$

$$k_n^- = \frac{24(n-1)^{2/3}D}{\lambda^2}\exp\left(-\frac{\delta g_n}{2k_BT}\right), \tag{12b}$$

where $\delta g_n$ is free energy of a cluster of $n+1$ molecules less than that of a cluster of $n$ molecules, $\lambda$ is the atom jump distance and $k_B$ is the Boltzmann constant, respectively.

The time-dependent cluster distribution is determined by the following coupled differential equations:

$$\frac{dN}{dt} = N_{n-1,t}k_{n-1}^+ - \left[N_{n,t}k_n^- + N_{n,t}k_n^+\right] + N_{n+1,t}k_{n-1}^-, \tag{13}$$

where $N_{n,t}$ is the number of clusters of $n$ molecules at a time $t$.

The finite difference method was employed to solve the above equations. The time was divided into a large number of small intervals, $\delta t$, and the number of clusters of $n$ molecules at the end of the interval, $N_{n,t+\delta t}$, is calculated by

$$N_{n,t+\delta t} = N_{n,t} + \delta t\left(dN_{n,t}/dt\right). \tag{14}$$

Substituting Eq. 13 into Eq. 14, one can get the following finite-difference equation:

$$\begin{aligned} N_{n,t+\delta t} = N_{n,t} + \delta t\Big(&N_{n-1,t}k_{n-1}^+ - \left[N_{n,t}k_n^- + N_{n,t}k_n^+\right] \\ &+ N_{n+1,t}k_{n-1}^-\Big). \end{aligned} \tag{15}$$

The initial distribution of clusters of different number of molecules can be defined by the Boltzmann distribution function as follows:

$$N_{n_0} = N_0 \cdot \exp\left(-\frac{\Delta F^*}{k_BT}\right), \tag{16}$$

where $N_{n_0}$ is the number of clusters of $n$ molecules at the initial time, $N_0$ is the density of nucleation points in the system and $\Delta F^*$ is the nucleation work of a clusters of $n$ molecules, respectively.

Theoretically, if the growth is continuous, this bimolecular reaction theory can describe the growth of large clusters as well. However, since the bimolecular reaction theory has a limitation of the cluster size and computer resources are finite, the evolution of such large clusters cannot be evaluated directly. Instead, an upper limit of the cluster size was set, and the growth of the cluster with a size larger than it was computed by using an approximate expression derived by Kelton et al. [23]:

$$g(r) = \frac{16D}{\lambda^2}\left(\frac{3\bar{v}}{4\pi}\right)^{1/3}\sinh\left[\frac{\bar{v}}{2k_BT}\left(\Delta G_v - \frac{2\sigma}{r}\right)\right]. \tag{17}$$

The determination of the physical parameters

In the present binary multiphase peritectic system, during the nucleation of a new phase, it is more difficult to determine the free energy change, $\Delta G$, as a function of temperature than to do so in a single phase system. By employing Thermo-calc™ software, the free energy change of each phase included in the peritectic reaction (liquid, $\eta$ and $\varepsilon$ phases) was calculated as a function of temperature and shown in Fig. 2.

Combining the calculated results with the phase diagram, we fitted the change of the volume free energy as a function of undercooling with a polynomial

$$\Delta G = a_1\Delta T' + a_2\Delta T'^2 + a_3\Delta T'^3, \tag{18}$$

where $\alpha_1$, $\alpha_2$ and $\alpha_3$ are constants.

According to Ref. [24], the interfacial energy was expressed as following:

$$\sigma = \sigma_0 + (T - T_0)(d\sigma/dT), \tag{19}$$

where $\sigma_0$, $T_0$ and $d\sigma/dT$ are thermodynamic constants.

The temperature-dependent diffusion coefficient was calculated from the Stokes–Einstein relation

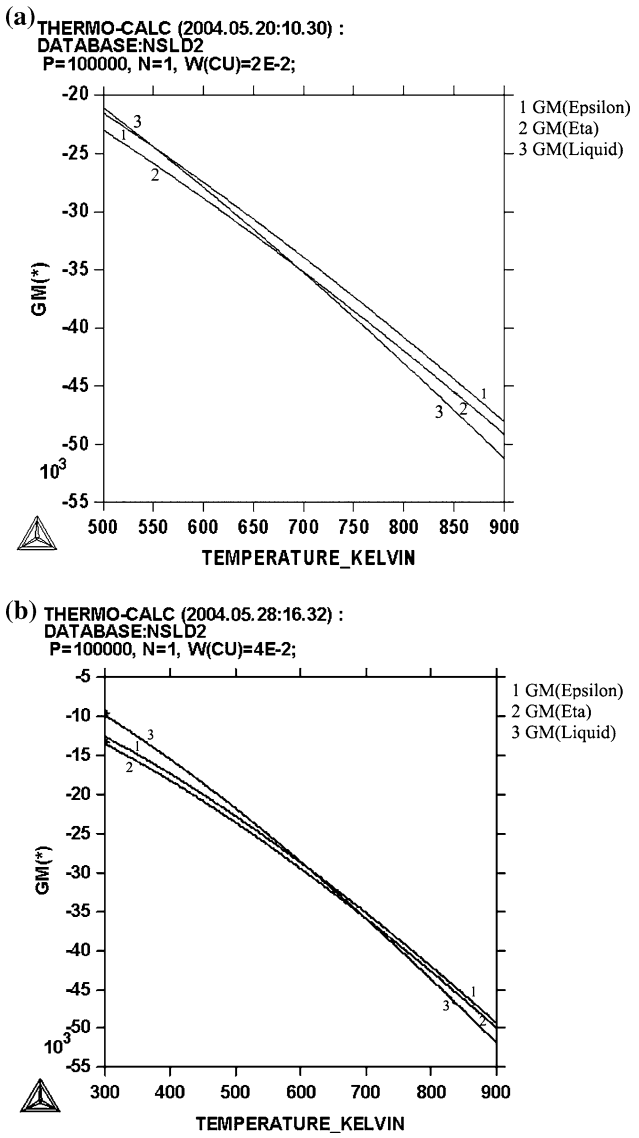


**Fig. 2** Free energy changes of liquid, ε and $\eta$ phases as a function of temperature calculated by Thermo-calc™ software in (**a**) Zn–2 wt.%Cu alloy and (**b**) Zn–4 wt.%Cu alloy, respectively

$$D = k_B/3\pi\alpha\eta, \tag{20}$$

where $\alpha$ is atom diameter, $\eta = \eta_0 \exp(E/RT)$ is the kinematic viscosity, $\eta_0$ and $E$ are physical constants, and $R$ is gas constant, respectively. The corresponding parameters were listed in Table 2.

## Results and discussions

### Time-dependent nucleation rate

Figure 3 shows the number of the ε crystal nuclei of a given size in front of the steady-growth interface of the $\eta$ phase under a solidification rate of 100 μm/s and a temperature gradient of 45 K/mm during unidirectional solidification of Zn–4.0 wt.%Cu alloy. It can be seen that each curve can be divided into two parts: linear and non-linear portions. The slope of each curve represents the nucleation rate of the corresponding phase. The non-linear behavior resulting from transient nucleation can be clearly observed. Since the linear portion of the curve corresponds to a steady-state nucleation rate, the transient time, $\tau_n^*$, can be determined by extrapolating the linear portion of the curve to the time axis. For crystal nuclei of a given size, the nucleation rate increases with the nucleation time till the threshold $\tau_n^*$ is reached and then keeps constant.

**Table 2** Parameters for Zn–Cu physical data of the phases involved

| Parameters | Symbol | Value | References |
|---|---|---|---|
| Volume free energy | $\alpha_1$ | 7.6802593 J/mol/K | Thermol-calc[1] |
| | $\alpha_2$ | 2.0328255 J/mol/K$^2$ | [24] |
| | $\alpha_3$ | 0.0033461 J/mol/K$^3$ | [24] |
| Interfacial energy | $\sigma_0$ | 7.82E–1 J/m$^2$ | [24] |
| | $d\sigma/dt$ | –1.7E–4 J/m$^2$/s | [24] |
| | $T_0$ | 692.15 K | [24] |
| Density | $\rho_{Cu}$ | $8.000 \times 10^3$ kg/m$^3$ | [24] |
| | $d\rho_{Cu}/dt$ | –0.801 kg/m$^3$/K | [24] |
| | $\rho_{Zn}$ | $6.575 \times 10^3$ kg/m$^3$ | [24] |
| | $d\rho_{Zn}/dt$ | –1.10 kg/m$^3$/K | [24] |
| Kinematic viscosity | $\eta_0$ | –3.19 K/wt.%Zn | [24] |
| | $E$ | 4,243 m/s | [24] |

[1] For 4 wt.%Cu alloy

### Incubation time

The total nucleation incubation time consists of the time lag of the nucleation process, $\tau^{\#}$, and the time spent by the clusters of the new phase on reaching a perceptible size, $\Delta t_p$. Thus total nucleation incubation time is

$$t_{inc} \cong \tau^{\#} + \Delta t_p. \tag{21}$$

As mentioned in the Section ''Transient nucleation model'', the nucleation of the new phase can be described as a non-isothermal crystallization process. Supposing that this process may start at any point with positive constitutional undercooling for the new phase, we can obtain a series of $t_{inc}$ and choose the shortest one as the actual incubation time. In the present model, first, the temperature and concentration fields were defined by numerically solving the coupled equations (1–8). Second, the constitutional undercooling for the new phase was calculated from the Eq. 9. Third, $\tau_n^*$ for crystal nuclei of the upper limit size was computed by numerically solving the Eq. 15. Fourth,

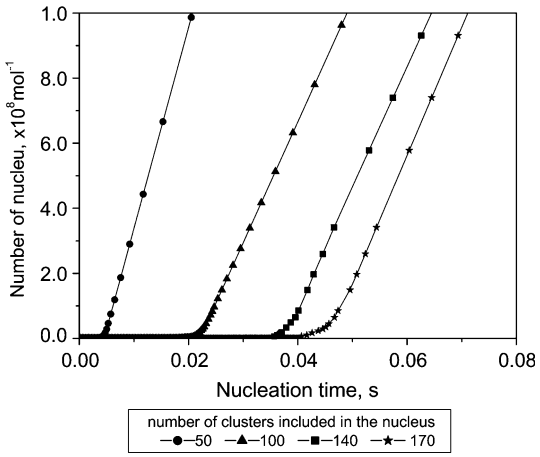


**Fig. 3** The computed distribution density of nucleus of a given size in a unidirectionally solidified Zn–4.0 wt.%Cu alloy with a solidification rate of 100 μm/s under temperature gradient of 45 K/mm

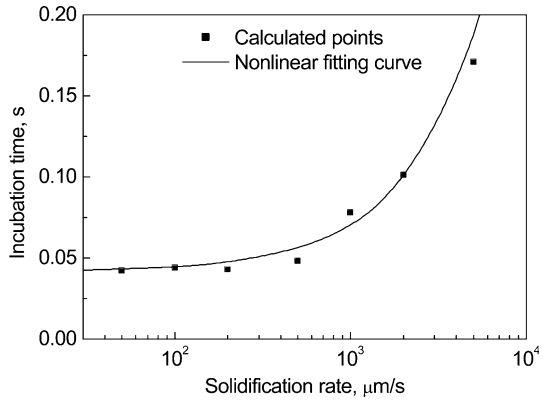


**Fig. 4** The computed incubation time of new phase in a unidirectionally solidified Zn–4.0 wt.%Cu alloy with various solidification velocities under temperature gradient of 45 K/mm and the non-linear fitting curve of the calculated points

$\Delta t_p$ was calculated from Eq. 17 and then $t_{inc}$ was determined by adding $\Delta t_p$ to $\tau_n^*$. Finally, after $t_{inc}$ of every point with positive constitutional undercooling for the new phase had been calculated, their minimum was chosen as the actual incubation time of the nucleation process. We should mention that the perceptible size employed here is 1 μm, which coincides with the value adopted in Ref. [18]. Furthermore, we found that the incubation time changes very slightly (about several percent) when the perceptible size varies from 0.1 to 1 μm, because the growth rate, $g(r)$ intensively increases with the nucleus size, $r$.

Figure 4 shows the calculated incubation time of the ε phase in front of the steady-growth interface of the $\eta$ phase under a temperature gradient of 45 K/mm during unidirectional solidification of Zn–4.0 wt.%Cu alloy. For exhibiting a clearer dependence of the incubation time on the solidification rate, the non-linear fitting curve of the calculated data was also plotted in this figure.

## Experimental results

Unidirectional solidification experiments on Zn–2.0 wt.%Cu hypoperitectic and Zn–4.0 wt.%Cu hyperperitectic alloys were carried out at withdrawal velocities varying from 1 to 6,400 μm/s in a Bridgman equipment under a high pure nitrogen atmosphere. A temperature gradient of 45 K/mm was employed in all these experiments. High-purity Zn(99.99%) and Cu(99.995%) were melted by the electric resistance melting method under high-purity argon atmosphere in a alumina crucible and cast into samples by the suction casting method. The diameter and the length of these samples are 1.8 and 150 mm, respectively. After the unidirectional solidification experiments, the samples were cut into longitudinal and transverse specimens. Each specimens was mounted, polished and etched for further analysis. The etchant was aqueous solution of $CrO_3$ and HCl (10 g $CrO_3$ plus 1.5 mL HCl in 100 mL de-ionized water). The metallographic observations were made at positions between 50 and 90 mm from the front end of the rods to ensure that the observed microstructures were in a steady state.

The optical micrographs of longitudinal sections in a Zn–2.0 wt.%Cu alloy growing at 10, 20 and 50 μm/s were shown in Fig. 5a–c, respectively. As shown in Fig. 5a, the typical microstructures at a velocity of 10 μm/s clearly consisted of dendrites (tree-like structures in Fig. 5a) and a featureless phase without any obvious microsegregation structures (the interdendritic phase in Fig. 5a) i.e. cells, dendrites, eutectic and so on. These tree-like structures were identified as ε dendrites, while the matrix was the planar interface structure of the $\eta$ phase [7, 8, 26]. The typical microstructures at a velocity of 20 μm/s are similar to those obtained at 10 μm/s, but the dendrites are less developed (as shown in Fig. 5b). It can be clearly seen that these ε dendrites are isolated and dispersed in the matrix of the $\eta$ phase. So these dendrites should not result from epitaxial growth but more possibly nucleation. As shown in Fig. 5c, when the solidification velocity increased to 50 μm/s, the ε dendrites disappeared and only the $\eta$ phase was observed. This $\eta$ phase obviously showed a cellular structure characteristic because the planar interface became instable and changed to cells with the increase of the solidification velocity. When the growth velocity increased further to 6,400 μm/s, these dendrites were never observed any more. In our previous paper [8], the constitutional undercooling for the ε phase in front of the steady-growth interface of the $\eta$ phase was calculated. The result clearly showed that the maximum constitutional undercooling was still much higher than the minimum nucleation undercooling predicted by the classic nucleation theory, even if

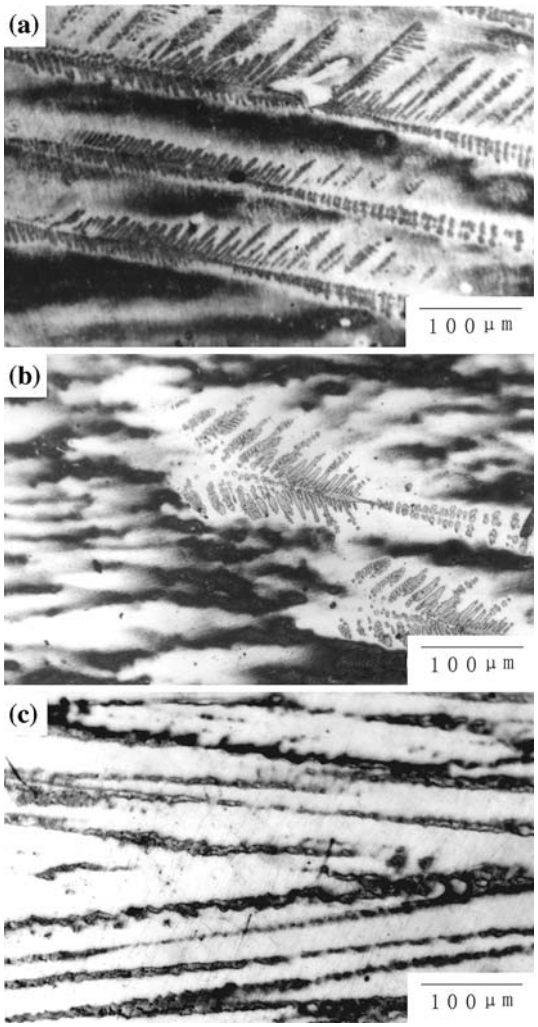


**Fig. 5** Microstructure of longitudinal section for Zn–2 wt.%Cu alloy investigated under unidirectional solidification velocities of (**a**) 10 μm/s, (**b**) 20 μm/s, (**c**) 50 μm/s, and the temperature gradient $G$ = 45 K/mm

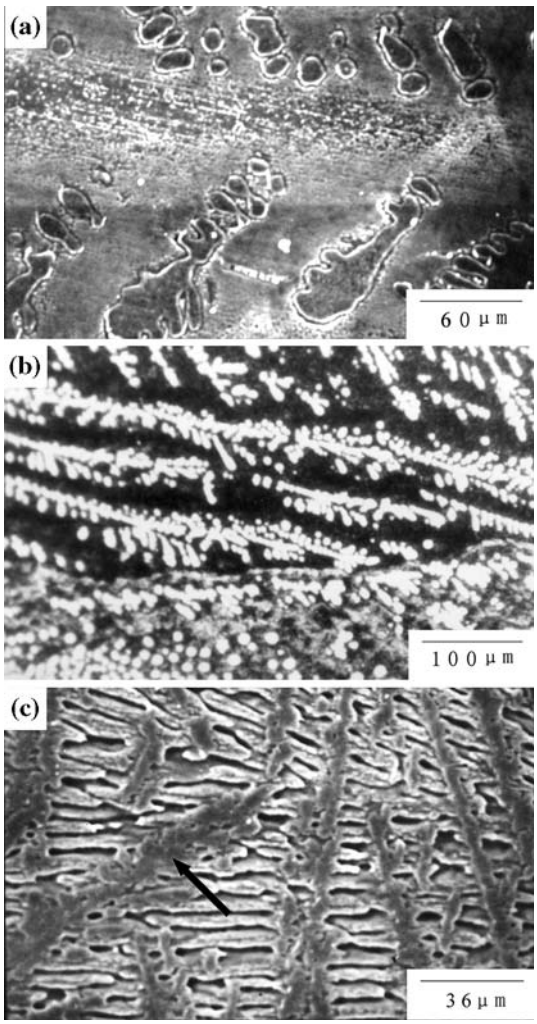


**Fig. 6** Microstructure of longitudinal section for Zn–4 wt.%Cu alloy investigated under unidirectional solidification velocities of (**a**) 10 μm/s, (**b**) 100 μm/s, (**c**) 1,600 μm/s, and the temperature gradient $G$ = 45 K/mm

the solidification velocity exceeded 50 μm/s much. Similar result was also reported by Ma et al. [7, 26]. That is to say, according to the classic nucleation theory, the ε phase should nucleate in the melt and consequently exist in the final solidification microstructures whether the solidification velocity is below 50 mm/s or not. But it obviously contradicts the experimental results.

Figure 6a–c show the typical microstructure of longitudinal sections in a Zn–4 wt.%Cu alloy at unidirectional solidification velocities of 10, 100 and 1,600μm/s, respectively. In Fig. 6a, tree-like gray structures can be clearly observed, which are ε dendrites dispersed in the matrix of the $\eta$ phase. These structures are similar to those of the Zn–2 wt.%Cu alloy grown at 10 and 20 μm/s, but relatively coarser. At a solidification velocity of 100 μm/s, as shown in Fig. 6b, the typical microstructures are also the $\eta$ phase and the ε dendrites. As the solidification velocity increased to 1,600μm/s, the ε dendrites (tree-like gray phase indicated by the black arrow in the figure) still existed, but the matrix changed to lamellar structures (as shown in Fig. 6c).

## Comparison with experimental results

Experimental measurements of the cluster-dependent growth velocity do not exist and for technical reason, it is not possible to directly measure the incubation time during unidirectional solidification so far. So a direct proof of the present model is not available. However, the nucleation behavior predicted by this model can be compared with the results obtained in unidirectional solidification experiments indirectly.

As mentioned in Section ''Incubation time'', it should take a certain time for a new phase to nucleate and coarsen even if the undercooling of the liquid phase is positive. During unidirectional solidification, the new phase can be observed in the final solidification structure only if the crystal nuclei of the new phase have grown to a perceptible size before the liquid/solid interface captures them, i.e. the ambient liquid phase solidifies. That is to say, the calculated incubation time, $t_{inc}$, should be shorter than the local solidification time based on the corresponding starting point, $t_s$, or else they will be captured by the solidification interface. So the present model can be connected to the experimental results by comparing $t_{inc}$ with $t_s$. If $t_{inc} < t_s$, the new phase (the ε phase) will exist in the final microstructure and vice versa. The local solidification period $t_{sj}$ of a point $j$ in front of the solid/liquid interface can be determined as follows:

$$t_{sj} = (z_j - z_i)/V_s, \tag{22}$$

where $z_j$ is the axial position of point $j$ in the moving coordinate system, $z_i$ is the axial position of the solid/liquid interface in the moving coordinate system, and $V_s$ is the solidification velocity, which is equal to the pulling velocity, $V_0$, under the steady-state condition.

According to the above expressing, the values of $t_s$ of the corresponding points in the Zn–2.0 wt.%Cu and Zn–4.0 wt.%Cu alloys at various unidirectional solidification velocities were calculated. Via comparing them with the values of $t_{inc}$ calculated by the present numerical model, one can predict whether the ε phase can be observed in the final microstructure or not at a given solidification velocity.

Figure 7 shows $t_{inc}$ of the ε phase and the corresponding $t_s$ in the Zn–2.0 wt.%Cu and Zn–4.0 wt.%Cu alloys at various unidirectional solidification velocities, respectively. For the Zn–2.0 wt.%Cu alloy, $t_{inc}$ is shorter than $t_s$ at a low solidification velocity. With the increase of solidification velocity, $t_{inc}$ increases and $t_s$ decreases quickly. While the solidification velocity exceeds about 30 μm/s, the former one will get ahead of the latter one. This indicates that the ε phase will not grow up to a perceptible size in front of the steady-growth $\eta$ interface at a unidirectional solidification velocity above 30 μm/s. That is to say, for the Zn–2.0 wt.%Cu alloy, the ε phase can only be observed in the final microstructure at a solidification velocity below 30 μm/s. This result shows an excellent agreement with the experimental results of this alloy. It can be seen that the present model reasonably explains the effect of the solidification velocity on the appearance of the ε dendrites in Bridgman solidification of the Zn–2.0 wt.%Cu alloy. For the Zn–4 wt.%Cu alloy, the present model predicts that $t_{inc}$ will outstrip $t_s$ at a solidification velocity above the threshold of about $2.8 \times 10^3$ μm/s. This means that the ε phase should not be observed in the final microstructure obtained at a solidification velocity above $2.8 \times 10^3$ μm/s. However, there are ε dendrites in the Bridgman sample at a solidification velocity even as high as $3.2 \times 10^3$ μm/s, which is a bit higher than the predicted threshold. We hold the viewpoint that besides possible impurity elements and the uncertainties of the thermophysical parameters, the most important reasons for this deviation should include the difference between the ideal conditions assumed in the present numerical model and the actual experimental condition, especially, convection currents usually existing in the liquid phase. As shown in the Zn–Cu binary phase diagram presented in Fig. 1, the liquidus slopes of both $\eta$ and ε phases are positive. During unidirectional solidification, as the solidification interface is advancing, component of Zn will be rejected by the solidification interface and then the concentration of Cu near the interface will be lower than that away from it. As a result, a concentration field in which the composition of Cu increases with the distance from the liquid/solid interface will be established. Because the solidification direction in our Bridgman experiments is upward and the Cu component has a larger density than Zn, a density current can be generated in the liquid phase upon the interface. It results in a spatial distribution of the crystal nuclei which is different from the convection-free condition assumed in the present numerical model. On the other hand, since the crystal nuclei of the ε phase have a higher density than the melt, these crystal nuclei will descend towards the interface. It makes the distribution density near the interface become higher than that predicted by the present numerical model and causes the decrease of the actual incubation time. However, since the difference between the results of calculation and the experiments is very slight, the calculated results are in reasonable agreement with those obtained by experiments.

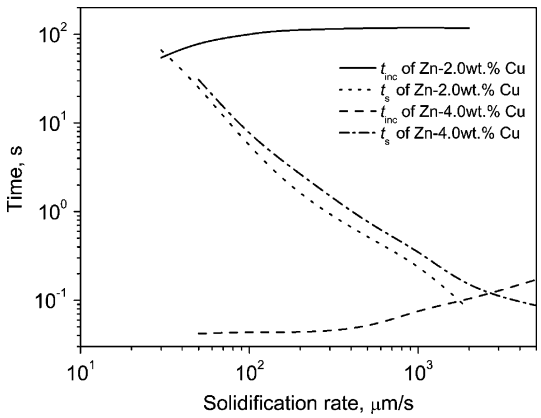


**Fig. 7** The comparison between the local solidification time, $t_s$ and the incubation time, $t_{inc}$ in unidirectional Zn–2.0 wt.%Cu and Zn–4.0 wt.%Cu alloys, respectively

## Conclusions

Based on the transient nucleation theory, a numerical model has been constructed to describe the nucleation of a new phase in front of the liquid–solid interface of a prior steady-growth phase in peritectic alloys with the combination of the concentration field calculated by a self-consistent numerical model for cellular/dendritic growth. The main results have been obtained as following:

1. The distribution density of the crystal nuclei of a given size in Zn rich Zn–Cu alloys non-linearly increases with nucleation time till the nucleation time reaches a threshold, and then increases approximately linearly.
2. For Zn–4.0 wt.% Cu alloys, the predicted incubation time changes very slightly when the unidirectional solidification rate increases from 50 to 500 μm/s, but it increases significantly when the solidification rate exceeds 500 μm/s.
3. The present model shows an excellent agreement with the results of the Bridgman experiments on the Zn rich Zn–Cu peritectic alloys. It reasonably explains the phenomenon that the ε dendrites in the matrix of the $\eta$ phase will disappear when the solidification velocity exceeds a certain value during unidirectional solidification of the above alloys. The calculated results also indicate the time-dependent characteristic of the formation of a new phase nucleating in front of the liquid–solid interface of a prior steady-growth phase.

**Acknowledgements** This work is financially supported by the National Natural Science Foundation of China Grant Nos. 50201012, 50471065 and National High Technology Research and Development Program of china No. 2002AA336050.

## References

1. Kohn A (1962) Mem Sci Rev Metall 59:713
2. Powell GLF, Colligan GA, Urquhart AW (1971) Metall Trans 2:918
3. Cisse J, Kerr HW, Bolling GF (1974) Metall Trans 5:713
4. Thoma J, Perepezko JH (1992) Metall Trans A 23:1347
5. Löser W, Volkmann T, Herlach DM (1994) Mater Sci Eng A 178:163
6. Eckler K, Herlach DM, Gärtner F, Assadi H, Norman AF, Greer AL (1997) Mater Sci Eng A 226–228:410
7. Ma D, Li Y, Ng SC, Jones H (2001) Sci Tech Adv Mat 2:127
8. Wang M, Su YP , Lin X, Huang WD (2003) Acta Metal Sin 39:838
9. Zeldovich YB (1943) Acta Phys (USSR) 18:1
10. Binder K, Stauffer D (1976) Adv Phys 25:343
11. Shneidman VA (1988) J Techn Phys (USSR) 58:2202
12. Gutzow I, Kashchlev D (1971) Advances in nucleation and crystallization of classes. American Ceramic Society, Columbus, OH, p 116
13. Gutzow I, Kashchiev D, Avramov I (1985) J Non-Cryst Solids 73:477
14. Gutzow I, Avramov I, Kästner K (1990) J Non-Cryst Solids 123:97
15. Gutzow I (1980) Contemp Phys 21:121
16. Löser W, Volkmann T, Herlach DM (1994) Mater Sci Eng A 178:163
17. Kelton KF (1993) J Non-Cryst 163:283
18. Massalski TB (1986) Binary alloy phase diagram. American Society for Metals, Metals Park, OH, p 235
19. Lin X, Li YM, Liu ZX, Li T, Huang WD (2001) Sci Techn Adv Mater 2:293
20. Lin X, Huang WD, Wang M, Li MY, Li T, Su YP, Shen SJ (2002) Sci China (Series E) 45:146
21. Massalski TB (1986) Binary alloy phase diagram. American Society for Metals, Metals Park, OH, p 75
22. Liu HY, Jones H (1992) Acta Metall 40:229
23. Cahn RW, Haasen P (1996) Physical metallurgy, 4th edn. North-Holland, Amsterdam, p 70
24. Gale WF, Totemeier TC (2004) Smithells metals reference book, 6th edn. Elsevier, Oxford, p 14.1
25. Kelton KF, Greer AL (1986) J Non-Cryst 79:295
26. Ma D, Li Y, Ng SC, Jones H (2000) Acta Mater 48:419